



Characterization of contaminant phases in foraminifera carbonates by electron microprobe mapping

L. D. Pena and I. Cacho

GRC Geociències Marines, Department of Stratigraphy, Paleontology and Marine Geosciences, University of Barcelona, C/ Martí i Franquès, s/n, E-08028 Barcelona, Spain (lpena@ub.edu)

E. Calvo

Institut de Ciències del Mar, CSIC, Passeig Marítim de la Barceloneta, 37–49, E-08003 Barcelona, Catalonia, Spain

C. Pelejero

Institut de Ciències del Mar, CSIC, Passeig Marítim de la Barceloneta, 37–49, E-08003 Barcelona, Catalonia, Spain

ICREA, CSIC, Passeig Marítim de la Barceloneta, 37–49, E-08003 Barcelona, Catalonia, Spain

S. Eggins and A. Sadekov

Research School of Earth Sciences, Australian National University, Canberra, Australian Capital Territory 0200, Australia

[1] The advent of new microanalytical techniques such as electron microprobe mapping (EMP) and laser ablation microsamplers coupled to mass spectrometers (LA-ICP-MS) provides a new array of possibilities to explore in great detail the trace elements distribution in foraminiferal carbonates. Here we apply these techniques to characterize diagenetic phases present in foraminiferal shells from Ocean Drilling Program Site 1240 in the Panama Basin, a region characterized by the presence of manganese-rich minerals in the sediments. The combined application of these techniques allows us to characterize the elemental and spatial distribution on the surface and across the foraminiferal shells. Results illustrate the presence of at least two different Mn-rich contaminant phases in the foraminiferal carbonates: Mn-rich carbonates and ferromanganese oxides. Elemental maps also highlight the relevance of the foraminifera shell texture and porosity in the distribution and formation of these contaminant phases. In the case of *Neogloboquadrina dutertrei*, Mn phases form a continuous thin layer in the inner part of the chambers, whereas for *Globigerinoides ruber*, Mn phases have a rather patchy distribution and are usually found within the pores. Significant high magnesium concentrations are always associated with these Mn-rich phases. These new findings support the need of removing these Mn-rich contaminant phases in order to measure accurately the Mg/Ca ratios in the foraminifera shell and therefore obtain reliable Mg/Ca paleotemperature reconstructions.

Components: 4560 words, 5 figures, 1 table.

Keywords: foraminifera; Mg/Ca; Ocean Drilling Program; electron microprobe; laser ablation; calcium carbonate.

Index Terms: 4825 Oceanography: Biological and Chemical: Geochemistry; 4875 Oceanography: Biological and Chemical: Trace elements (0489); 4954 Paleooceanography: Sea surface temperature.

Received 4 March 2008; **Revised** 17 May 2008; **Accepted** 4 June 2008; **Published** 15 July 2008.

Pena, L. D., I. Cacho, E. Calvo, C. Pelejero, S. Eggins, and A. Sadekov (2008), Characterization of contaminant phases in foraminifera carbonates by electron microprobe mapping, *Geochem. Geophys. Geosyst.*, 9, Q07012, doi:10.1029/2008GC002018.

1. Introduction

[2] Knowledge of trace element distributions in foraminiferal carbonate obtained with microanalytical techniques has substantially improved our understanding of trace elements as paleoenvironmental proxies [Anand and Elderfield, 2005; Sadekov et al., 2008]. Tools such as secondary ion mass spectrometry (SIMS) [Allison and Austin, 2003; Bice et al., 2005; Kunioka et al., 2006] and especially laser ablation inductively coupled plasma–mass spectrometry (LA-ICP-MS) and electron microprobe mapping (EMP) [Eggins et al., 2003, 2004; Hathorne et al., 2003; Reichart et al., 2003; Sadekov et al., 2005; Toyofuku and Kitazato, 2005; Wu and Hillaire-Marcel, 1995] have been particularly useful in this regard. Both LA-ICP-MS and EMP have proved to be a valuable source of information in constraining the paleoecology of planktonic [Eggins et al., 2003, 2004; Sadekov et al., 2005] and benthic foraminifera [Toyofuku and Kitazato, 2005]. Pena et al. [2005] have further applied the LA-ICP-MS compositional depth profiling technique to identify Mn-Mg-rich contaminant phases and to assess the efficiency of different cleaning protocols for measuring the Mg/Ca ratios of foraminiferal tests. That study documented evidence for the presence of Mn-rich contaminant phases and identified the Mn-rich carbonate, kutnahorite. The present study goes one step further by using EMP mapping to characterize the spatial distribution and extent of Mn-Mg-rich contaminant phases within foraminifera tests. This approach provides new insight into the nature and formation of these phases, and is a powerful tool for diagnosing contamination problems and ensuring the effectiveness of the applied cleaning protocols prior to trace element analysis.

2. Regional Setting

[3] The samples selected for this study are from Ocean Drilling Program (ODP) Site 1240, Leg 202 (0° 01.31'N, 86° 27.76'W and 2921 m of water depth) located at the northern flank of the Carnegie ridge in the Panama Basin. This basin is characterized by typical sediments that are especially rich in manganese minerals. This is partially caused by

the level of biological productivity in the region, which is among the highest found in the oceans [Moore et al., 1973]. The strong upwelling conditions are also accompanied by hydrothermal activity, resulting in the supply of relatively large amounts of both biogenic reactive organic carbon and hydrothermal manganese to the seafloor [Aller, 1990]. Additional dissolved manganese comes through relatively unaltered seawater flow in the underlying basement which has been well constrained in regions of the central equatorial Pacific [Baker et al., 1991]. The high organic carbon supply to the bottom enhances the consumption of oxygen, and results in oxygen depletion within a few centimeters of the sediment-water interface [Pedersen and Price, 1982; Reimers, 1987]. These conditions promote manganese reduction reactions and the total estimated annual flux of carbon can apparently be oxidized [Aller, 1990]. The dissolution of manganese oxides in deeper sediments under reducing conditions results in an upward diffusion of dissolved Mn²⁺ ions and reprecipitation of Mn⁴⁺ as oxides where higher redox potentials exist, usually near the sediment-water interface [Pedersen and Price, 1982]. Under anoxic conditions the maximum dissolved manganese concentration in interstitial pore waters is typically limited by the precipitation of manganese carbonates. Authigenic Mn-carbonate phases have been previously identified in sediments from the Panama Basin [Boyle, 1983; Pedersen and Price, 1982] and further confirmed and characterized [Pena et al., 2005].

3. Experimental Setup

[4] Two different planktonic foraminifera species (*N. dutertrei* and *G. ruber*) were handpicked from five sediment samples selected from within a Mn-rich interval at Site 1240 where kutnahorite-like minerals were identified to be present within foraminifera tests [Pena et al., 2005]. The selected interval is of Pleistocene age (128.07 ka and 128.52 ka), corresponding with the penultimate deglaciation (Termination II) and accordingly with the isotopic stratigraphy available for Site 1240 [Pena et al., 2008]. Bulk sediments were wet sieved (>63 μm) with distilled water and dried. The sampling of foraminifera for analysis was

Table 1. ODP Site 1240 Samples Selected for Analyses

Sample	Foraminifera Species	Depth ^a (mcd)	Age (ka)	Average Mg/Ca ^b (mmol/mol)	Average Mn/Ca ^b (mmol/mol)
D022	<i>Neogloboquadrina dutertrei</i>	14.79	128.52	1.65	0.58
D031	<i>Neogloboquadrina dutertrei</i>	14.75	128.07	2.66	7.74
R021	<i>Globigerinoides ruber</i>	14.79	128.52	4.56	2.59
R022	<i>Globigerinoides ruber</i>	14.79	128.52	3.51	1.98
R023	<i>Globigerinoides ruber</i>	14.79	128.52	4.68	3.15

^aMeters composite depth.

^bAveraged ratios from laser profiles in uncleaned samples.

performed under microscope inspection in the 315–355 μm fraction, separating individuals of the two selected species for both EMP and LA-ICP-MS analysis. Foraminifera tests for EMP analysis were mounted in epoxy resin and polished to expose foraminifera test walls in cross section following the methodology of *Eggins et al.* [2004]. Table 1 summarizes the labeling of samples and their description.

[5] We used a Cameca SX-100 electron microprobe to generate element distribution maps for Ca, Mg, Mn and Fe within cross-sections of planktonic foraminifera walls. These analyses were performed at the Research School of Earth Sciences (RSES), the Australian National University, where this technique had been applied previously to foraminifera carbonates [*Eggins et al.*, 2004; *Sadekov et al.*, 2005]. The Cameca SX-100 was operated in Wavelength Dispersive Spectrometry (WDS) mode with different $K\alpha$ X-ray lines for each element and using four spectrometers and three different spectrometer crystals (PET, TAP and LLIF) to simultaneously measure the elements Ca (PET), Mg (TAP), Mn (LLIF) and Fe (LLIF). Small excitation volumes were achieved by setting up the column conditions with an accelerating voltage of 20 kV and a beam current of 20 nA. The selected areas were mapped using a 1 μm step size and 0.5 s dwell time. The results are illustrated as maps of relative measured intensities (counts per second) for the different elements within foraminifera wall cross sections. Where Ca intensities have fallen below 3000 cps (as compared to 5000 cps in “pure” foraminiferal carbonate) values have been assumed to be zero in order to delineate and remove “edge effects” that are encountered with EMP analysis [*Sadekov et al.*, 2005]. In view of difficulty in accurately calibrating EMP intensity maps to elemental concentrations [e.g., *Eggins et al.*, 2004; *Sadekov et al.*, 2005], we have chosen to

present our results as simple element intensity maps. These are a highly valuable tool that clearly show contaminant distribution patterns in foraminiferal carbonates and avoid misinterpretations that can otherwise arise from incorrectly calibrated elemental concentrations.

[6] The LA-ICP-MS compositional depth profiling technique used in this work was also carried out at the RSES, the Australian National University, and has been comprehensively described by [*Eggins et al.*, 2003, 2004] and later applied by [*Pena et al.*, 2005] to identify contaminant phases and assess the efficiency of cleaning protocols on foraminiferal tests. The laser ablation system comprises a pulsed ArF Excimer laser ($\lambda = 193 \text{ nm}$), coupled to an Agilent 7500 s quadrupole mass spectrometer via a custom built laser ablation cell and sample transport system. Layers of uniform diameter ($\sim 30 \mu\text{m}$) and thickness ($\sim 0.1 \mu\text{m}$) are ablated from foraminifera shell surfaces with each laser pulse, at a pulse repetition rate of 4 Hz and relatively low laser fluence of 4 J/cm^2 . The custom built ablation cell was designed to minimize particulate residence times ($t_{1/2} \sim 0.35\text{s}$) and thereby provide submicron depth resolution. The material ablated from progressively deepening ablation pits was transported via a mixed Ar-He gas flow to the ICP-MS. Five isotopes (three trace elements) were simultaneously measured by repeated, rapid sequential peak hopping (1 point/peak, dwell time = 10–30 ms) between selected isotopes (^{24}Mg , ^{25}Mg , ^{43}Ca , ^{44}Ca and ^{55}Mn), for a total mass cycle time of <200 ms. The ICP-MS was optimized for sensitivity across the analyte mass range and also for low molecular species production (by maintaining $\text{ThO}^+/\text{Th}^+ < 0.5\%$). Data reduction from raw time resolved spectra involves screening of spectra for outliers, followed by subtraction of mean background intensities (measured with the laser off), and then calibration of instrument re-

sponse to the NIST610 glass standard reference material.

4. Results and Discussion

[7] The *N. dutertrei* EMP results show a characteristic element distribution pattern across foraminifera shell walls (Figures 1a–1n), with the presence of a relatively Ca-rich inner layer that is also enriched in Mg and particularly in Mn but without traces of Fe. These results indicate that this inner layer is composed of a Mn-Mg-rich carbonate as opposed to Fe-Mn oxides. The presence of a Mn-Mg-rich carbonate was previously identified by means of X-ray diffraction as kutnahorite (Ca(Mn, Mg)(CO₃)₂) in the same sediment samples [Pena et al., 2005]. Detailed inspection of the element maps indicates the presence of some Fe rich areas infilling the outermost pores of the foraminifera shell (Figures 1d and 1k). These pore fillings are also associated with relatively high Mg values but not with high Mn levels. The intensity ratios for these elements relative to calcium (Figures 1e–1g and 1i–1n) further confirm these observations.

[8] Laser ablation-ICP-MS element profiles obtained from the same samples provide a more quantitative picture that confirms the presence and character of this inner carbonate layer which has Mg/Ca ratios up to ~6 mmol/mol and Mn/Ca ratios up to ~25 mmol/mol (Figure 2). These results are in agreement with previous data reported by [Pena et al., 2005] for the mineral kutnahorite. The laser profiles extend for differing lengths which correspond to the thickness of the different foraminifera chamber walls. In all cases, they confirm a consistent pattern of relatively constant Mg/Ca and Mn/Ca values through the shell, with rapid and parallel increase in both elemental ratios at the innermost part of the chamber wall. There are significant differences between the average ratios of the different foraminifera chambers, ranging between ~1 mmol/mol and ~6 mmol/mol in Mg/Ca and from “normal” values of Mn/Ca up to 25 mmol/mol at the inner wall. The origin of the different internal Mg/Ca and Mn/Ca ratio values of the different

foraminifera chambers have been discussed at length in previous studies [Eggins et al., 2003; Sadekov et al., 2005]. It is interesting to note from the EMPs shown herein that the inner Mn-Mg rich carbonate layer appears to be weakly attached to the actual foraminiferal carbonate. The Ca maps show the existence of gaps and void space separating these compositionally distinct carbonates (Figures 1a and 1h), and supporting the diagenetic nature of this inner layer. Despite the presence of the inner diagenetic coating, the original shell chemistry seems to be well preserved (Figure 2b) and therefore may maintain its original Mg/Ca ratio which could be measured after removal of the coatings. A previous study of these samples addressed the efficiency of different cleaning protocols in removing these contaminant layers [Pena et al., 2005], and proposed that the removal of kutnahorite-like minerals during the “reductive” cleaning step may result from a higher susceptibility of these thin layers compared to the foraminifera wall calcite. The new EMP maps presented here show that this inner thin layer of diagenetic calcite is weakly attached to the foraminiferal wall (Figures 1f and 1m) which may favor the removal of this layer either by mechanical (foraminifera crushing and/or ultrasonication) or by chemical (reductive) means during the cleaning protocols performed for trace elements analyses. The Pena et al. [2005] study also proposed the potential presence of manganese oxides (MnO_x) between the foraminiferal shell and the diagenetic calcite and that their dissolution during the “reductive” cleaning step could promote the removal and/or dissolution of the kutnahorite layers. In this regard, Figure 1g suggests the presence of relatively high Fe/Ca ratios between the *N. dutertrei* shell and the diagenetic layers that might indicate the presence of Fe-Mn oxides; however, this most likely is an edge effect artifact due to the low Ca intensities in this region of the shell.

[9] The EMP maps of *G. ruber* wall sections show different element distribution patterns that can also be associated with the presence of contaminant phases within the foraminifera shell (Figures 3

Figure 1. Electron microprobe elemental mappings of two *N. dutertrei* individuals (D022 and D031; see Table 1 for detailed information) on an exposed section of the foraminifera shell. (a–d, h–k) Distribution of calcium, magnesium, manganese, and iron in the foraminifera test. (e–g, l–n) Intensity ratios of Mg/Ca, Mn/Ca, and Fe/Ca distributions. All intensity values are expressed in counts per second (cps) as shown in the color bars. The counting statistics uncertainty (2σ) ranges from ~3% (Ca) to ~15–25% (Mn, Mg, and Fe). The accompanying SEM images show the polygons selected for elemental mapping and yellow arrows pointing toward the inner Mn-rich layers. Also note the scale bars for size reference.

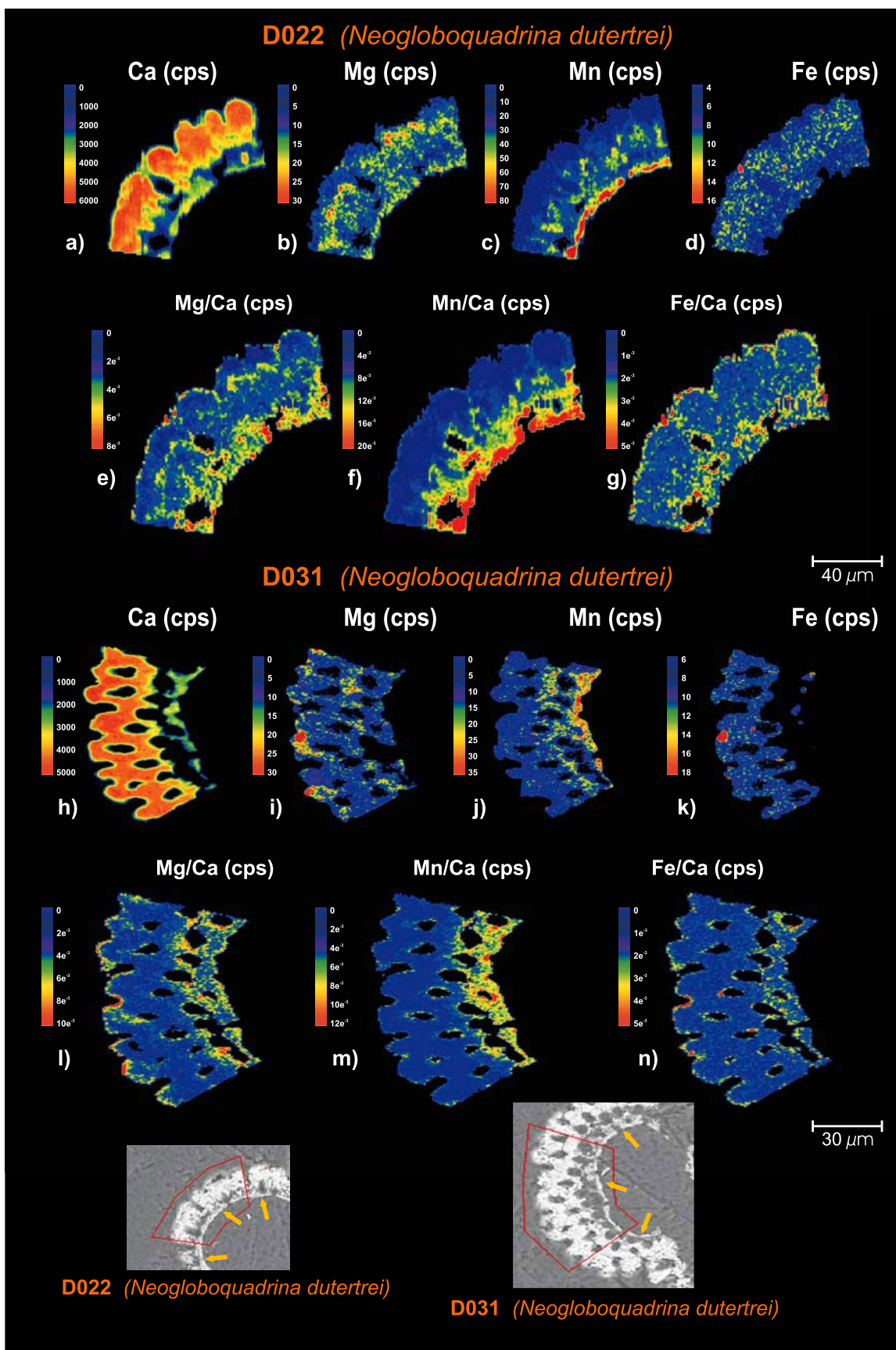


Figure 1

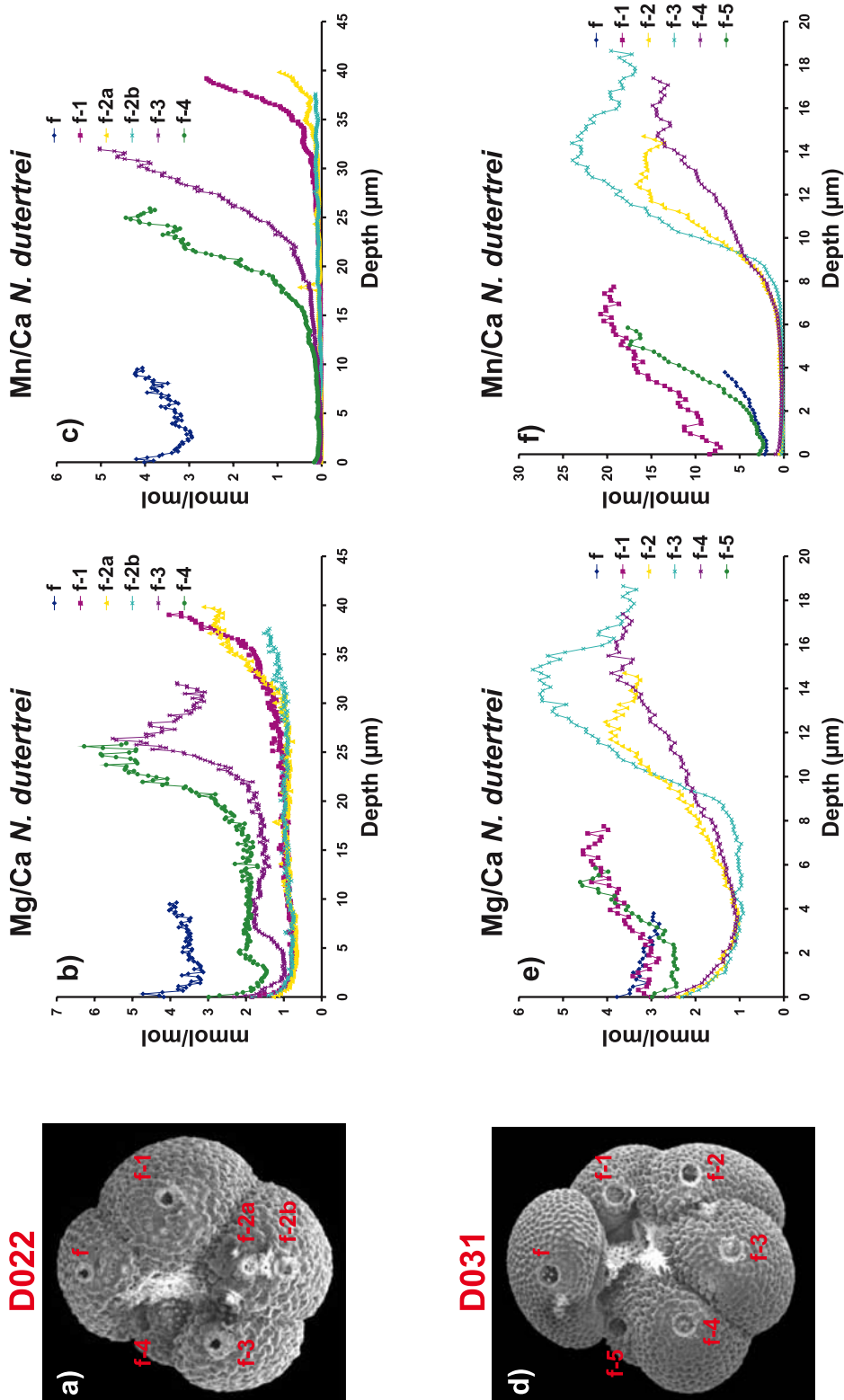


Figure 2. Laser ablation ICP-MS profiles from two representative *N. dutertrei* individuals (D022 and D031; see Table 1 for detailed information). Colored profiles were assigned to correlative chambers, ordered from the last (youngest) to the first (oldest) chamber in *N. dutertrei* individuals (i.e., f is the last formed chamber, and f-5 is the first). Elemental ratios are expressed in mmol/mol, and depth profiles are expressed in μm. (a and d) SEM images from the selected individuals showing the corresponding laser ablation pits. (b and e) Mg/Ca versus depth profiles of different laser-ablated chambers. (c and f) Mn/Ca versus depth profiles of different laser-ablated chambers.

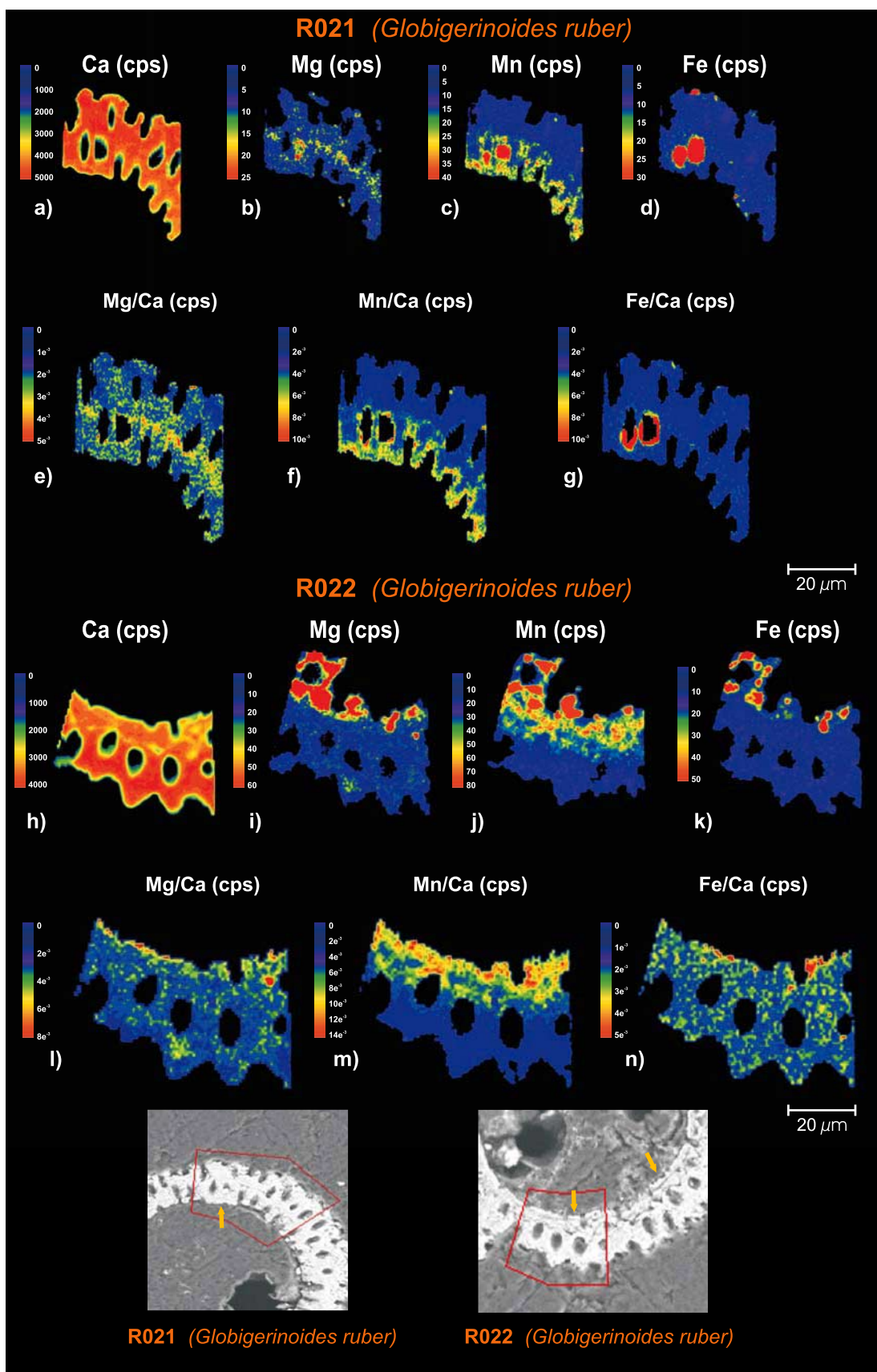


Figure 3

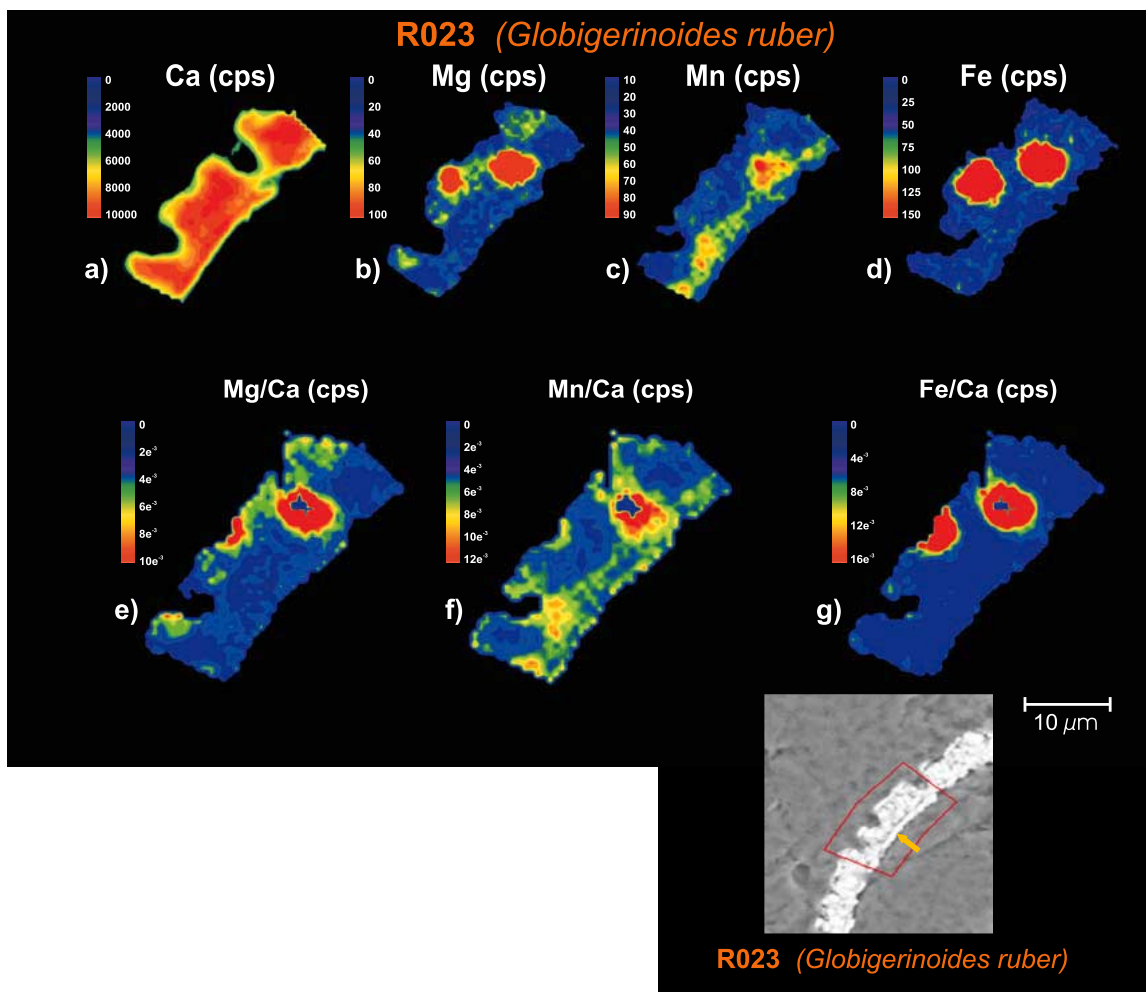


Figure 4. Electron microprobe elemental mappings of one *G. ruber* individuals (R023; see Table 1 for detailed information) on an exposed section of the foraminifera shell. (a–d) Distribution of calcium, magnesium, manganese, and iron in the foraminifera test. (e–g) Intensity ratios of Mg/Ca, Mn/Ca, and Fe/Ca distributions. All intensity values are expressed in counts per second (cps) as shown in the color bars. The counting statistics uncertainty (2σ) ranges from $\sim 3\%$ (Ca) to $\sim 15\text{--}25\%$ (Mn, Mg, and Fe). The accompanying SEM image show the polygons selected for elemental mapping and yellow arrows pointing toward the inner Mn-rich layers. Also note the scale bars for size reference.

and 4). In *G. ruber*, Mn enrichment also occurs preferentially at the inner part of the foraminifera shell walls but their chemical and physical properties are significantly different than described above for *N. dutertrei* (Figures 3e–3f, 3l, 3m, 4e, and 4f). Unlike in *N. dutertrei* the Mn-rich calcite layer is not de-attached from the main foraminifera car-

bonate. In addition, Fe is concentrated around pore margins located near the inner shell wall (Figure 3k) and further within the foraminifera wall (Figures 3d and 4d). These Fe-rich “hot spots” are also characterized by high Mn and Mg intensities but low or absent Ca counts (Figures 3a–3d and 3h–3k) as shown by the element intensity

Figure 3. Electron microprobe elemental mappings of two *G. ruber* individuals (R021 and R022; see Table 1 for detailed information) on an exposed section of the foraminifera shell. (a–d, h–k) Distribution of calcium, magnesium, manganese, and iron in the foraminifera test. (e–g, l–n) Intensity ratios of Mg/Ca, Mn/Ca, and Fe/Ca distributions. All intensity values are expressed in counts per second (cps) as shown in the color bars. The counting statistics uncertainty (2σ) ranges from $\sim 3\%$ (Ca) to $\sim 15\text{--}25\%$ (Mn, Mg, and Fe). The accompanying SEM images show the polygons selected for elemental mapping and yellow arrows pointing toward the inner Mn-rich layers. Also note the scale bars for size reference.

ratios maps (Figures 3e–3g, 3l–3n, and 4e–4g). As a consequence, we are able to identify two different contaminant phases in these *G. ruber* samples. First is a Mn-Mg rich carbonate which is not restricted to a thin inner wall layer but has a more heterogeneous and penetrative presence within the foraminifera wall. The second is more likely to be Mn-Fe oxide phase(s) that are always associated to high Mg values. Laser ablation-ICP-MS profiles confirm the lack of well defined inner Mn-Mg rich carbonate layers in *G. ruber* and show a considerable spread in the average element ratio compositions of the individual chambers, ranging from 3.3 to 4.7 mmol/mol for Mg/Ca and from 2.0 to 3.1 mmol/mol for Mn/Ca (Figures 5a–5i). These ratio values are low compared to those associated with the “kutnahorite” inner layer in the *N. dutertrei* samples. But, on the other hand, *G. ruber* Mn/Ca ratios are always higher than those recorded by the true foraminifer calcite in *N. dutertrei*. Because laser ablation pits are about 30 μm diameter they incorporate several pores and spine holes in each profile measurement, and consequently are an average of the true foraminifera shell and any contaminants contained within the ablated pores, which may include both Fe-Mn oxides and Mn-Mg carbonates. The fact that these contaminant phases occur pervasively within the foraminifera porosity (Figures 3d–3k and 4d), rather than as an homogeneous layer at the inner side of the chamber, makes them difficult to discriminate by the laser ablation technique. However, the electron microprobe mapping clearly identifies the location of these Fe-Mn oxides within the foraminifera shell, especially their association with pores. This explains both the heterogeneous laser profiles that are often obtained for *G. ruber* and the rather erratic pattern recorded in the laser profiles for this species. The elimination of these contaminant phases by the standard cleaning protocols developed for trace element measurements may also be difficult and this could explain why the Mn/Ca ratios of *G. ruber* show generally higher background levels than those of *N. dutertrei* after cleaning [Pena et al., 2005]. In the case of *N. dutertrei*, its porosity is less penetrative and the contaminant phases are homogeneously distributed

in a thin layer near the inner part of the shell, which allows for more efficient removal during cleaning.

[10] These new results highlight the value of characterizing the chemical nature of contaminant phases attached to foraminifera shells that have the potential to compromise accurate proxy reconstructions based on elemental ratios (i.e., Mg/Ca). The results we have presented demonstrate that all Mn-rich phases are associated to high Mg values and, consequently, that it is necessary to completely remove or at least significantly reduce the levels of the Mn-rich contaminant phases in order to obtain reliable paleotemperature reconstructions. In this regard, the application of LA-ICP-MS in samples cleaned through different protocols demonstrated that Mn-enriched phases could be satisfactorily removed by the inclusion of the so-called “reductive step” in the cleaning protocol [Pena et al., 2005]. However, the application of this step has co-lateral implications since it also induces partial dissolution of the actual foraminiferal calcite and thereby can cause further decrease in measured Mg/Ca ratios [Boyle, 1981; Brown and Ederfield, 1996; Martin and Lea, 2002; Rosenthal et al., 2000]. Some studies have argued in favor of the elimination of this cleaning step in order to avoid this partial dissolution [Yu et al., 2007]. Our results indicate that the elimination of the “reductive” step could enhance significantly the error of temperature reconstructions since measurements would include the Mn-Mg-rich contaminant phases. We accordingly would argue that the intensive cleaning is needed and the associated problem of preferential dissolution of high Mg foraminifera shell components can be addressed by using regional species specific Mg/Ca calibrations that would compensate for the offset in the Mg/Ca ratios introduced by the reductive cleaning [Rosenthal et al., 2004]. Alternatively, the development of a less aggressive reductive chemical step could avoid problems deriving from foraminiferal calcite dissolution with existing cleaning protocols [Yu et al., 2007].

5. Summary

[11] Both electron microprobe mapping and laser ablation-ICP-MS depth profiling have provided

Figure 5. Laser ablation ICP-MS profiles from three representative *G. ruber* individuals (R021, R022, and R023; see Table 1 for detailed information). Colored profiles were assigned to correlative chambers, ordered from the last (youngest) to the first (oldest) chamber in *N. dutertrei* individuals (i.e., f is the last formed chamber, and f-5 is the first). Elemental ratios are expressed in mmol/mol, and depth profiles are expressed in μm . (a, d, and g) SEM images from the selected individuals showing the corresponding laser ablation pits. (b, e, and h) Mg/Ca versus depth profiles of different laser-ablated chambers. (c, f, and i) Mn/Ca versus depth profiles of different laser-ablated chambers.

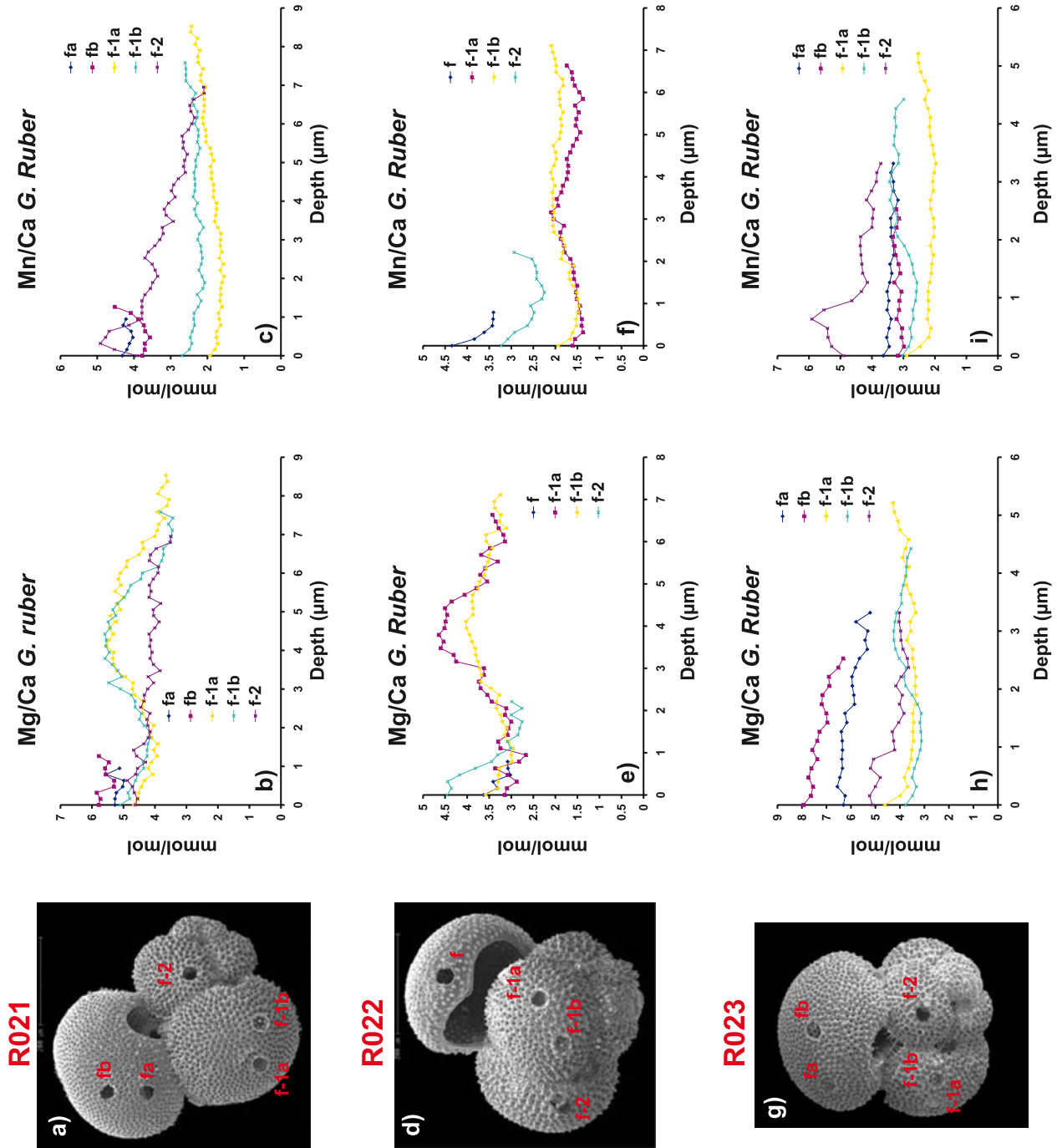


Figure 5

new insights into the nature of Mn-rich contaminant phases found in planktonic foraminifera carbonates from the Panama Basin. Our results demonstrate the occurrence of at least two different Mn-rich contaminant phases that are also rich in Mg. The element map distributions reveal these phases are most likely to be Mn-Mg rich carbonates, potentially kutnahorite-like minerals, and Fe-Mn oxides. The distribution of these minerals is strongly linked to shell architecture, with more porous species (*G. ruber*) having more abundant contaminant phase development within pores, and less-porous species (*N. dutertrei*) as thin layers at the inner surface of shell walls. These differences in the spatial distribution of these mineral phases control the different Mn/Ca background levels detected between these two species after the application of trace element cleaning protocols [Pena *et al.*, 2005]. Our results clearly illustrate the importance of applying appropriate cleaning protocols in order to produce reliable past temperature reconstructions for the ocean using Mg/Ca paleothermometry. This study highlights the importance of both identifying the chemical composition and physical location of different contaminant phases and demonstrates that LA-ICP-MS and EMP are highly valuable tools in this regard.

Acknowledgments

[12] L.P. and I.C. acknowledge a fellowship from the Comer Abrupt Climate Change Foundation (USA). Funding for this research was also provided by the Natural Environment Research Council through UK-ODP. This work was supported in part by the Spanish Ministry of Science and Innovation through project ROMIAT (CTM2006-01957/MAR). E.C. and I.C. also acknowledge support through a Ramón y Cajal contract from the Spanish Ministry of Education and Science. Roger Heady and Sally Stowe (Electron Microscope Unit at the Australian National University) are thanked for their assistance in obtaining SEM images. This research used samples provided by the ODP. The ODP is sponsored by the NSF and participating countries under management of Joint Oceanographic Institutions (JOI), Inc. We thank all three reviewers and the associate editor for their very helpful comments and suggestions.

References

- Aller, R. C. (1990), Bioturbation and manganese cycling in hemipelagic sediments, *Philos. Trans. R. Soc. London, Ser. B*, *331*, 51–68, doi:10.1098/rsta.1990.0056.
- Allison, N., and W. E. N. Austin (2003), The potential of ion microprobe analysis in detecting geochemical variations across individual foraminifera tests, *Geochem. Geophys. Geosyst.*, *4*(2), 8403, doi:10.1029/2002GC000430.
- Anand, P., and H. Elderfield (2005), Variability of Mg/Ca and Sr/Ca between and within the planktonic foraminifers *Globigerina bulloides* and *Globorotalia truncatulinoides*, *Geochem. Geophys. Geosyst.*, *6*, Q11D15, doi:10.1029/2004GC000811.
- Baker, P. A., P. M. Stout, M. Kastner, and H. Elderfield (1991), Large-scale lateral advection of seawater through oceanic crust in the central equatorial Pacific, *Earth Planet. Sci. Lett.*, *105*, 522–533, doi:10.1016/0012-821X(91)90189-0.
- Bice, K. L., G. D. Layne, and K. Dahl (2005), Application of secondary ion mass spectrometry to the determination of Mg/Ca in rare, delicate, or altered planktonic foraminifera: Examples from the Holocene, Paleogene, and Cretaceous, *Geochem. Geophys. Geosyst.*, *6*, Q12P07, doi:10.1029/2005GC000974.
- Boyle, E. A. (1981), Cadmium, zinc, copper, and barium in foraminifera tests, *Earth Planet. Sci. Lett.*, *53*, 11–35, doi:10.1016/0012-821X(81)90022-4.
- Boyle, E. A. (1983), Manganese carbonate overgrowths on foraminifera tests, *Geochim. Cosmochim. Acta*, *47*, 1815–1819, doi:10.1016/0016-7037(83)90029-7.
- Brown, S. J., and H. Elderfield (1996), Variations in Mg/Ca and Sr/Ca ratios of planktonic foraminifera caused by postdepositional dissolution: Evidence of shallow Mg-dependent dissolution, *Paleoceanography*, *11*, 543–551, doi:10.1029/96PA01491.
- Eggins, S., P. De Deckker, and J. Marshall (2003), Mg/Ca variation in planktonic foraminifera tests: Implications for reconstructing palaeo-seawater temperature and habitat migration, *Earth Planet. Sci. Lett.*, *212*, 291–306, doi:10.1016/S0012-821X(03)00283-8.
- Eggins, S., A. Sadekov, and P. De Deckker (2004), Modulation and daily banding of Mg/Ca in *Orbulina universa* tests by symbiotic photosynthesis and respiration: A complication for seawater thermometry?, *Earth Planet. Sci. Lett.*, *225*, 411–419, doi:10.1016/j.epsl.2004.06.019.
- Hathorne, E. C., O. Alard, R. H. James, and N. W. Rogers (2003), Determination of intratest variability of trace elements in foraminifera by laser ablation inductively coupled plasma-mass spectrometry, *Geochem. Geophys. Geosyst.*, *4*(12), 8408, doi:10.1029/2003GC000539.
- Kunioka, D., K. Shirai, N. Takahata, Y. Sano, T. Toyofuku, and Y. Ujiie (2006), Microdistribution of Mg/Ca, Sr/Ca, and Ba/Ca ratios in *Pulleniatina obliquiloculata* test by using a NanoSIMS: Implication for the vital effect mechanism, *Geochem. Geophys. Geosyst.*, *7*, Q12P20, doi:10.1029/2006GC001280.
- Martin, P. A., and D. W. Lea (2002), A simple evaluation of cleaning procedures on fossil benthic foraminiferal Mg/Ca, *Geochem. Geophys. Geosyst.*, *3*(10), 8401, doi:10.1029/2001GC000280.
- Moore, T. C., Jr., G. R. Heath, and R. O. Kowsmann (1973), Biogenic sediments of the Panama Basin, *J. Geol.*, *81*, 458–472.
- Pedersen, T. F., and N. B. Price (1982), The geochemistry of manganese carbonate in Panama Basin sediments, *Geochim. Cosmochim. Acta*, *46*, 59–74, doi:10.1016/0016-7037(82)90290-3.
- Pena, L. D., E. Calvo, I. Cacho, S. Eggins, and C. Pelejero (2005), Identification and removal of Mn-Mg-rich contaminant phases on foraminiferal tests: Implications for Mg/Ca past temperature reconstructions, *Geochem. Geophys. Geosyst.*, *6*, Q09P02, doi:10.1029/2005GC000930.
- Pena, L. D., I. Cacho, P. Ferretti, and M. A. Hall (2008), ENSO-like variability during glacial terminations and interlatitudinal teleconnections, *Paleoceanography*, doi:10.1029/2008PA001620, in press.
- Reichart, G.-J., F. Jorissen, P. Anschutz, and P. R. D. Mason (2003), Single foraminiferal test chemistry records the mar-

- ine environment, *Geology*, *31*, 355–358, doi:10.1130/0091-7613(2003)031<0355:SFTCRT>2.0.CO;2.
- Reimers, C. E. (1987), An *in situ* microprofiling instrument for measuring interfacial pore water gradients: Methods and oxygen profiles from the North Pacific Ocean, *Deep Sea Res., Part A*, *34*, 2019–2035, doi:10.1016/0198-0149(87)90096-3.
- Rosenthal, Y., G. P. Lohmann, K. C. Lohmann, and R. M. Sherrell (2000), Incorporation and preservation of Mg in *Globigerinoides sacculifer*: Implications for reconstructing the temperature and $18\text{O}/16\text{O}$ of seawater, *Paleoceanography*, *15*, 135–145, doi:10.1029/1999PA000415.
- Rosenthal, Y., et al. (2004), Interlaboratory comparison study of Mg/Ca and Sr/Ca measurements in planktonic foraminifera for paleoceanographic research, *Geochem. Geophys. Geosyst.*, *5*, Q04D09, doi:10.1029/2003GC000650.
- Sadekov, A. Y., S. M. Eggins, and P. De Deckker (2005), Characterization of Mg/Ca distributions in planktonic foraminifera species by electron microprobe mapping, *Geochem. Geophys. Geosyst.*, *6*, Q12P06, doi:10.1029/2005GC000973.
- Sadekov, A., S. M. Eggins, P. De Deckker, and D. Kroon (2008), Uncertainties in seawater thermometry deriving from intratest and intertest Mg/Ca variability in *Globigerinoides ruber*, *Paleoceanography*, *23*, PA1215, doi:10.1029/2007PA001452.
- Toyofuku, T., and H. Kitazato (2005), Micromapping of Mg/Ca values in cultured specimens of the high-magnesium benthic foraminifera, *Geochem. Geophys. Geosyst.*, *6*, Q11P05, doi:10.1029/2005GC000961.
- Wu, G., and C. Hillaire-Marcel (1995), Application of LP-ICP-MS to benthic foraminifers, *Geochim. Cosmochim. Acta*, *59*, 409–414, doi:10.1016/0016-7037(94)00370-2.
- Yu, J., H. Elderfield, M. Greaves, and J. Day (2007), Preferential dissolution of benthic foraminiferal calcite during laboratory reductive cleaning, *Geochem. Geophys. Geosyst.*, *8*, Q06016, doi:10.1029/2006GC001571.